Fluid transport in Antarctic sea ice

K. M. Golden[1*], A. Gully[1], and J. L. Tison[2]

[1]University of Utah, Department of Mathematics
155 S 1400 E RM 233, Salt Lake City, UT 84112-0090 USA

[2]Laboratoire de Glaciologie, CP 160/03, Université Libre de Bruxelles
50, av. F. D. Roosevelt, 1050 - Bruxelles, Belgium

[*]To whom correspondence should be addressed; E-mail: golden@math.utah.edu.

Fluid flow through porous sea ice mediates a broad range of processes which are critical to predictions of climate change, and the response of polar ecosystems. We have made the first measurements of fluid permeability in Antarctic pack ice, and find that the granular sea ice there leads to strikingly different fluid transport behavior than in the Arctic. In particular, granular ice exhibits a percolation threshold, the on−off switch for fluid transport, for brine volume fractions around 10% or higher, rather than 5% observed in columnar ice. Tracer experiments on extracted sea ice blocks further support these results. Our findings shed new light on key processes such as snow-ice formation, melt pond evolution, CO_2 exchanges, and nutrient replenishment, and their parameterizations in global climate and biogeochemical models.

The polar sea ice packs form a key component of Earth's climate system, and are sensitive indicators of climate change (*1, 2*). They also host extensive algal and bacterial communities which sustain life in the polar oceans (*1, 3*). While global climate models generally predict declines in polar sea ice, they have significantly underestimated the dramatic losses observed in the summer Arctic ice pack (*4, 5*). On the other hand, Antarctic sea ice has increased overall, along with some significant regional losses (*6, 7*).

Our focus here is on key sea ice processes which must be better understood to improve the predictions of climate models and the future of the polar ice packs, as well as the microbial

communities that live there. In particular, fluid flow through porous sea ice helps control the evolution of melt ponds and ice pack albedo (*8*), brine drainage and the evolution of salinity profiles (*9, 10*), snow-ice formation, where sea water floods the ice surface and then freezes (*11, 12*), ocean-ice-atmosphere CO_2 exchanges (*13*), convection-enhanced thermal transport (*14, 15*), and biomass build-up fueled by nutrient fluxes (*1, 3, 16, 17*). For example, it is believed that ice-albedo feedback has played a significant role in the declines observed in the Arctic (*18*). Snow-ice formation, on the other hand, may have helped in thickening the Antarctic sea ice pack (*11, 12*), and may become more important in the Arctic with increased precipitation and thinning ice, so that it is more susceptible to flooding.

The fluid permeability of sea ice, which depends strongly on its brine microstructure, plays a key role in understanding such processes, and in parameterizing them in large-scale models. To date, columnar microstructures have received disproportionate attention, mostly due to their prevalence in Arctic sea ice and their importance in undisturbed ice growth (*9, 10, 19*). However, granular microstructures, which lack intragranular inclusions and exhibit a film of brine enveloping individual grains, are particularly important for processes which are relevant to climate studies. For example, granular ice is common in surface layers in the Arctic (*20, 21*), which directly underly the melt ponds controlling ice albedo. Examination of the crystalline structure in sea ice from a recent trans-Arctic survey (*21*) showed a striking increase in overall granular ice fraction, of just over 40% compared to previous observations of around 10% (*22*). In the Antarctic it has long been observed that granular ice (*11, 23–25*), accounts for a fraction of up to around 40% of the sea ice pack. Snow-ice in particular, with granular microstructure itself, accounts for over a quarter of the ice found in the Southern Ocean, with much higher fractions in some regions (*26*). An accurate accounting of sea ice processes involving fluid flow in climate and biogeochemical models relies on knowledge of the fluid permeability of granular ice.

In (*27*) it was observed that for brine volume fractions ϕ below about 5%, columnar sea

ice is effectively impermeable to fluid flow, yet is increasingly permeable for ϕ above 5%. For a typical bulk salinity of 5 ppt, this critical brine volume fraction $\phi_c \approx 5\%$ corresponds to a critical temperature $T_c \approx -5^\circ$ C, which is known as the *rule of fives*. The critical brine volume fraction was explained in terms of the *percolation threshold* in a continuum model for compressed powders which was has been used to understand the behavior of stealthy or radar absorbing materials. In (*28*) a comprehensive theory for the vertical fluid permeability $k(\phi)$ of columnar sea ice was developed, and validated experimentally with laboratory and Arctic field data. Micro-scale imaging methods based on X-ray computed tomography (CT) and pore structure analysis were also developed to provide detailed pictures of the brine microstructure and the evolution of its connectivity with temperature (*28, 29*).

During September and October of 2007, we measured the fluid permeability of first year Antarctic pack ice as participants in the Australian Sea Ice Physics and Ecosystem Experiment (SIPEX), aboard the icebreaker *Aurora Australis*. The study area was located off the coast of East Antarctica, between 115° E and 130° E, and 64° S and 66° S. Permeability measurements were made at 8 of the 15 ice stations along the cruise track of the *Aurora*, and we obtained 38 data points covering a range of depths, temperatures, salinities, and ice types. Full length cores were taken nearby by our colleagues, usually within a few meters of our location, and were later subjected to crystallographic and other analyses. When we separated out the permeability data which was likely being influenced primarily by granular microstructures, we found that the critical threshold for fluid flow had effectively doubled to around $\phi_c \approx 10\%$. For a typical salinity of around 5 ppt, the corresponding critical temperature is around $T_c \approx -2.5^\circ$ C (*30*). Moreover, as predicted by our percolation theoretic analysis in (*28*), we find here that the *universal* lattice critical exponent of about 2 for columnar ice in the Arctic still accurately describes the take-off of $k(\phi)$ above the threshold ϕ_c for granular sea ice in the Antarctic.

We also extracted blocks of sea ice with a chain saw, turned them upside down, and

poured cooled tracers into shallow channels cut into the top surface of the block (which is actually the sea ice bottom). Thin vertical slices were cut from blocks, which exposed the fluid fronts, layers of different microstructures, and brine channels. The tracers easily penetrated a highly permeable bottom layer, but stopped when the fluid reached a depth characterized by a brine volume fraction of about 10%.

The novel behavior we find in the percolation threshold for fluid transport in granular ice is explained in terms of the compressed powder model (*31, 32*). By measuring the relative dimensions of the ice grains and the fluid inclusions in photomicrographs of granular sea ice, we obtain a percolation threshold of around 10%, with the possibility of even higher thresholds for more finely grained microstructures.

We consider low Reynolds number flow of brine of viscosity η through sea ice. The volume fractions of brine and ice are ϕ and $1-\phi$. The velocity and pressure fields in the brine satisfy the Stokes equations for incompressible fluids. Under appropriate assumptions (*33*), the homogenized velocity $\mathbf{v}(\mathbf{x})$ and pressure $p(\mathbf{x})$ satisfy Darcy's law and the incompressibility condition for the velocity,

$$\mathbf{v} = -\frac{1}{\eta}\,\mathbf{k}\,\nabla p, \qquad \nabla \cdot \mathbf{v} = 0, \tag{1}$$

where $\mathbf{k}$ is the permeability tensor, with vertical permeability $\mathrm{k}_{zz} = k$ in units of m^2.

The *in situ* permeability data was collected using a hydrological bail test (*34*), where partial cylindrical holes were drilled vertically into the sea ice, and the cores removed. As water filled the hole, equilibrating to a known freeboard level, time series measurements of the height $h(t)$ of the rising water column or hydraulic head were taken, with h in meters (m) and t in seconds (s). The permeability of the ice underneath the borehole can be accurately estimated using the equation

$$h(t) = h(t_0)e^{-k_{exp}t(g\rho/\eta L)}, \tag{2}$$

with measured permeability k_{exp} (m^2), ice thickness beneath the borehole L (m), density

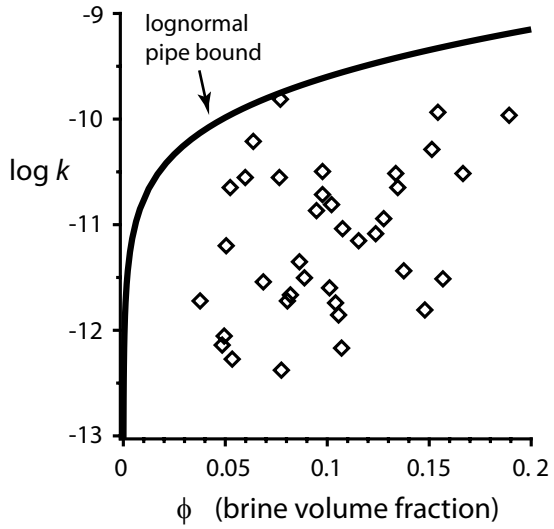

Figure 1: Comparison of *in situ* data on the vertical fluid permeability k (m^2) of Antarctic sea ice (37 diamonds) with a rigorous upper bound.

ρ (kg m^{-3}), gravitational constant g (m s^{-2}), and initial time t_0. To obtain the vertical component k of the permeability, the data were corrected in two ways, using calculations in (*34*). First, we excluded the contribution from horizontal flow through the cylindrical sides of the holes, assuming a 10:1 ratio of vertical to horizontal flow in sea ice (*34*). Then, based on simulations of the fluid pressure field in the ice (*34*), we estimated the flow through the bottom of the hole due exclusively to upward vertical flow directly beneath the hole, yielding our measurements of the vertical permeability k of sea ice.

Rigorous bounds on bulk properties of composites, such as sea ice, provide benchmarks which are useful in assessing data, and in connecting effective behavior to mixture geometry (*33*). In previous work (*28, 35*) we found rigorous upper bounds for k based on an observed lognormal distribution for the horizontal cross-sectional areas A of of the brine inclusions (*20*). In this case $Z = \ln A$ has a normal probability density with mean μ and variance σ^2,

$$P(Z) = \frac{1}{\sqrt{2\pi\sigma^2}}\, e^{-(Z-\mu)^2/2\sigma^2}. \tag{3}$$

The cross-sectional radius $a(\phi) = 7 \times 10^{-5} + (1.6 \times 10^{-4})\phi$ m increases according to mea-

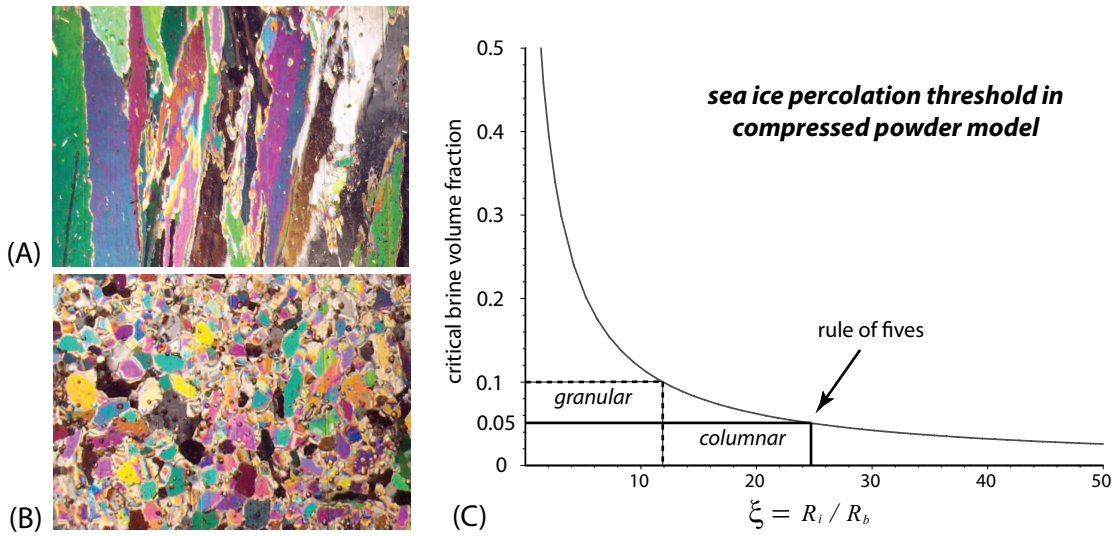

Figure 2: (A) Columnar and (B) granular microstructures. (C) Percolation threshold in the compressed powder model as a function of the ratio of the particle radii.

surements of pore sizes with temperature (*20, 36*). The bound is a special case of optimal void bounds (*33, 37*), and takes the form

$$k(\phi) \leq \frac{\phi}{8\pi} \langle A(\phi) \rangle \, e^{\sigma^2}. \tag{4}$$

With variance $\sigma^2 \approx 1$ and $\langle A(\phi) \rangle = \pi a^2(\phi)$ as above (*20*), the *lognormal pipe bound* in (4) captures all our field data, as shown in Figure 1 (one data point where no fluid influx was measured is not shown on the logarithmic scale).

Based on previous analyses of Arctic columnar sea ice (*28*), we expected to see similar threshold behavior near a 5% critical brine volume fraction in Antarctic sea ice as well. However, initial analysis of our permeability data did not show the expected behavior – the threshold appeared to be "smeared out," or stretched over a range of ϕ. Elementary analysis of the compressed powder model (*31*) we used to explain the rule of fives (*27*) shows that granular microstructures should display higher thresholds than columnar ice. As water flows back into the hole, even a thin layer of granular ice beneath it can determine the effective threshold behavior. Given the significant presence of granular ice in our samples,

we separated the permeability data into two categories, those with primarily columnar ice under the bottom of the hole, and those with even a small amount (roughly a quarter) or more of granular ice under the hole. An image of the polycrystalline microstructure of Antarctic columnar ice under cross-polarization is shown in Figure 2 (A), and an image of granular ice is shown in (B). These samples were taken in the Bellingshausen Sea in October 2007 during the Sea Ice Mass Balance in the Antarctic (SIMBA) experiment.

In order to estimate the percolation threshold ϕ_c for fluid transport in Antarctic granular ice, we use a compressed powder model (*27, 31*). In this model, large polymer spheres of radius R_p are mixed with much smaller metal spheres of radius R_m, and then the mixture is compressed. The main parameter controlling the threshold is the ratio $\xi = R_p/R_m$. An approximate formula for the critical volume fraction for percolation of the small metal spheres is given by $\phi_c = (1 + \xi\theta/(4X_c))^{-1}$, where θ is a reciprocal planar packing factor, and X_c is a critical surface area fraction of the larger particles which must be covered for percolation by the smaller particles (*31*). Values based on microstructural analysis giving good agreement with experiments are $X_c = 0.42$ and $\theta = 1.27$. This mixture geometry is roughly similar to the ice-brine microstructure of sea ice, where the ice grains have radius R_i and the brine inclusions have radius R_b (or half the thickness of a brine film enveloping an ice grain), with $\xi = R_i/R_b$ in this case. We have estimated a range of ξ values from photomicrographs of granular microstructures, and obtained a representative value of around $\xi \approx 12$, leading to a threshold value of around $\phi_c \approx 10\%$, as illustrated in Figure 2 (C). We remark that fine-grained columnar ice which displays geometric similarity to classic granular ice can also exhibit these higher percolation threshold values, and that even finer grained frazil microstructures will likely have even higher thresholds.

Percolation theory (*33, 38, 39*) has been used to model transport in disordered materials where the connectedness of one phase, like brine in sea ice, dominates the effective behavior. Consider the square ($d = 2$) or cubic ($d = 3$) network of bonds joining nearest neighbor sites

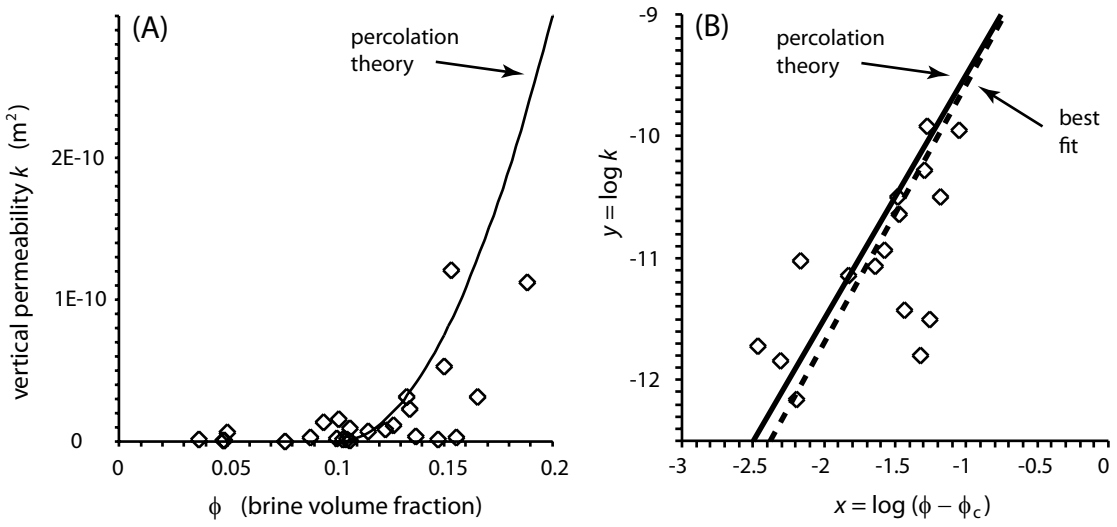

Figure 3: Comparison of *in situ* data on k (m^2) for Antarctic sea ice with percolation theory, displayed on a linear scale in (A) and on a logarithmic scale in (B), where a statistical best fit (dotted line) of the data is shown along with the prediction of percolation theory with $\phi_c \approx 0.1$.

on the integer lattice $\mathbb{Z}^d$. The bonds are assigned fluid conductivities $\kappa_0 > 0$ (open) or 0 (closed) with probabilities p and $1-p$. There is a critical probability p_c, $0 < p_c < 1$, called the *percolation threshold*, where an infinite, connected set of open bonds first appears. In $d = 2$, $p_c = \frac{1}{2}$, and in $d = 3$, $p_c \approx 0.25$. Let $\kappa(p)$ be the permeability of this random network in the vertical direction. For $p < p_c$, $\kappa(p) = 0$. For $p > p_c$, near the threshold $\kappa(p)$ exhibits power law behavior, $\kappa(p) \sim \kappa_0(p - p_c)^e$ as $p \to p_c^+$, where e is the permeability critical exponent. For lattices, e is believed to be *universal*, depending only on d, and is equal to t, the lattice electrical conductivity exponent (*33, 38–40*). In $d = 3$, it is believed (*33*) that $t \approx 2.0$, and there is a rigorous bound (*39*) that $t \leq 2$.

Although e can take non-universal values in the continuum, it was shown in that for lognormally distributed inclusions the behavior is universal, with $e \approx 2$. The scaling factor k_0 is estimated using critical path analysis and microstructural observations (*28*). Thus

$$k(\phi) \sim 3\,(\phi - \phi_c)^2 \times 10^{-8}\ \mathrm{m}^2, \quad \phi \to \phi_c^+, \tag{5}$$

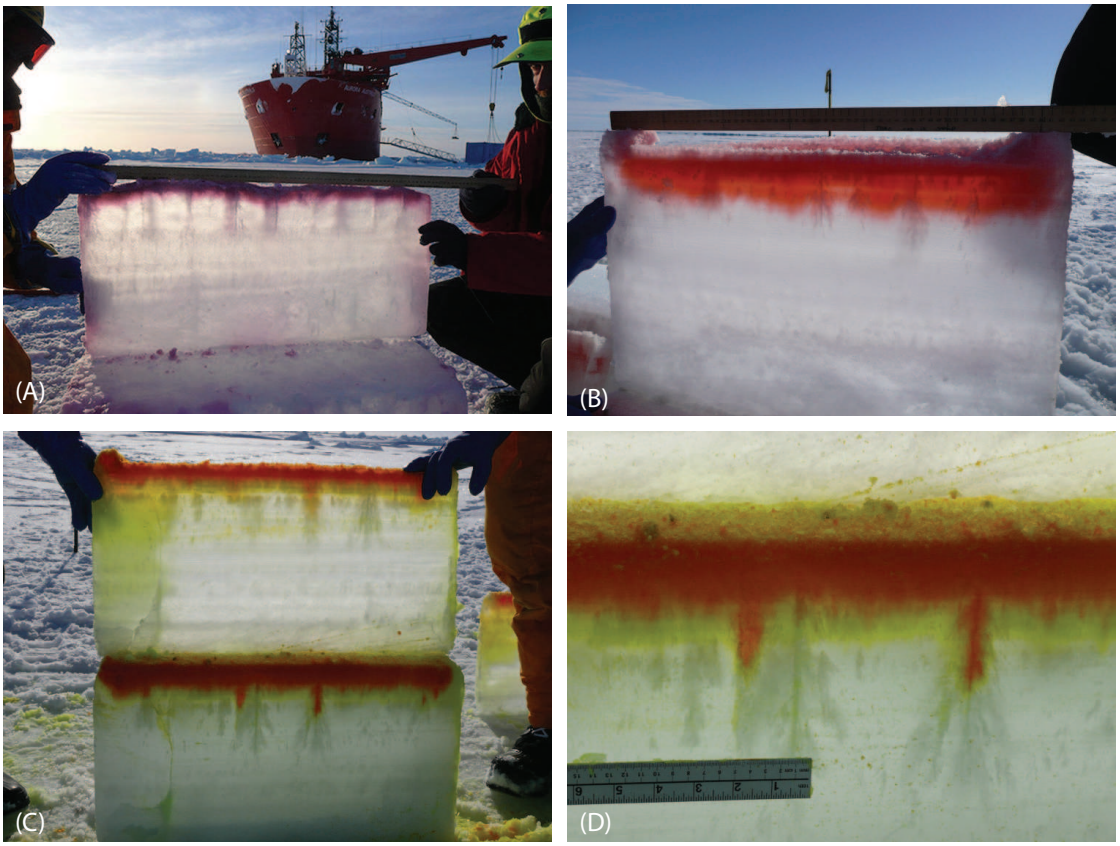

Figure 4: Penetration of tracers into inverted blocks of sea ice. The fluid penetrated about 5 cm into the ice in (A), about 10 cm in (B), and about 9 cm in (C) and (D). In each case the descending fluid passed through an initial layer a few centimeters deep of highly permeable ice of average brine volume fraction in the range 18.5% - 21.5%, until reaching relatively impermeable ice with brine volume fraction of about 10%, where it stoppped flowing. In (A), the temperature and brine volume decreased more rapidly, and the tracer stopped after 5 cm. In (B) and (C) the 10% brine volume threshold was located about 10 cm down, and in (D) a tracer plume was also able to descend deeper through a large brine channel.

with $\phi_c \approx 0.1$ for granular ice. In Figure 3 (A), we display the granular permeability data along with the curve in (5). In (B) we show in logarithmic variables the percolation theory prediction along with a statistical best fit, for permeability data with ϕ above 0.10, showing close agreement.

In Figure 4 the results of our tracer experiments are shown, where we poured fluid tracers into inverted sea ice blocks. In each case the fluid descended through a layer of highly permeable sea ice, and stopped when it reached colder, impermeable granular ice (or fine-grained columnar ice) of brine volume fraction around 10%. These experiments vividly demonstrated the critical threshold for fluid transport in Antarctic sea ice.

References and Notes

1. D. N. Thomas, G. S. Dieckmann, eds., *Sea Ice: An Introduction to its Physics, Chemistry, Biology and Geology* (Blackwell, Oxford, 2003).

2. M. C. Serreze, M. M. Holland, J. Stroeve, *Science* **315**, 1533 (2007).

3. C. H. Fritsen, V. I. Lytle, S. F. Ackley, C. W. Sullivan, *Science* **266**, 782 (1994).

4. J. Stroeve, M. M. Holland, W. Meier, T. Scambos, M. Serreze, *Geophys. Res. Lett.* **34**, L09591, doi: 10.1029/2007GL029703 (2007).

5. J. Boé, A. Hall, X. Qu, *Nature Geoscience* (online, 15 March, 2009).

6. H. J. Zwally, J. C. Comiso, C. L. Parkinson, D. J. Cavalieri, P. Gloersen, *J. Geophys. Res.* **107**, 3041, doi:10.1029/2000JC000733 (2002).

7. J. Zhang, *J. Climate* **20**, 2515 (2007).

8. H. Eicken, T. C. Grenfell, D. K. Perovich, J. A. Richter-Menge, K. Frey, *J. Geophys. Res. (Oceans)* **109**, C08007.1 (2004).

9. W. F. Weeks, S. F. Ackley, *The Geophysics of Sea Ice*, N. Untersteiner, ed. (Plenum Press, New York, 1986), pp. 9–164.

10. H. Eicken, *Sea Ice: An Introduction to its Physics, Chemistry, Biology and Geology*, D. N. Thomas, G. S. Dieckmann, eds. (Blackwell, Oxford, 2003), pp. 22–81.

11. T. Maksym, M. O. Jeffries, *J. Geophys. Res.* **105**, 26,313 (2000).

12. D. C. Powell, T. Markus, *J. Geophys. Res. C (Oceans)* **110**, C06001, doi:10.1029/2003JC002212 (2005).

13. S. Rysgaard, J. Bendtsen, L. T. Pedersen, H. Ramløv, R. N. Glud, *J. Geophys. Res.* **114**, C09011, doi:10.1029/2008JC005088 (2009).

14. V. I. Lytle, S. F. Ackley, *J. Geophys. Res.* **101**, 8853 (1996).

15. H. J. Trodahl, *et al.*, *J. Geophys. Res.* **105**, 11347 (2000).

16. M. P. Lizotte, K. R. Arrigo, eds., *Antarctic Sea Ice: Biological processes, interactions and variability* (American Geophysical Union, Washington D.C., 1998).

17. H. Eicken, *Polar Biol.* **12**, 3 (1992).

18. D. K. Perovich, J. A. Richter-Menge, K. F. Jones, B. Light, *Geophys. Res. Lett.* **35**, L11501, doi:10.1029/2008GL034007 (2008).

19. B. Light, G. A. Maykut, , T. C. Grenfell, *J. Geophys. Res.* **108**, 3051 (2003).

20. D. K. Perovich, A. J. Gow, *J. Geophys. Res.* **101**, 18,327 (1996).

21. D. K. Perovich, *et al.*, *J. Geophys. Res.* **114**, C00A04, doi:10.1029/2008JC004892 (2009).

22. W. B. T. III, A. J. Gow, D. A. Meese, H. W. Bosworth, E. Reimnitz, *J. Geophys. Res.* **104**, 1489 1504, doi:10.1029/98JC02607 (1999).

23. M. O. Jeffries, R. A. Shaw, A. L. V. K. Morris, H. R. Krouse, *Antarctica, J. Geophys. Res.* **99**, 985 (1994).

24. A. P. Worby, R. A. Massom, *Res. Rep.* **7** (1995). Antarctic CRC.

25. H. Eicken, *Antarctic Sea Ice Physical Processes, Interactions and Variability*, M. O. Jeffries, ed. (AGU Antarctic Res. Ser., 1998), vol. 74, pp. 89–122.

26. T. Maksym, T. Markus, *J. Geophys. Res.* **113**, C02S12, doi:10.1029/2006JC004085 (2008).

27. K. M. Golden, S. F. Ackley, V. I. Lytle, *Science* **282**, 2238 (1998).

28. K. M. Golden, *et al.*, *Geophys. Res. Lett.* **34**, L16501 (6 pages and issue cover), doi:10.1029/2007GL030447 (2007).

29. D. J. Pringle, J. E. Miner, H. Eicken, K. M. Golden, Pore-space percolation in sea ice single crystals. *J. of Geophys. Res. C*, in press.

30. G. Frankenstein, R. Garner, *J. Glaciol.* **6**, 943 (1967).

31. R. P. Kusy, *J. Appl. Phys.* **48**, 5301 (1977).

32. R. P. Kusy, D. T. Turner, *Nature* **229**, 58 (1971).

33. S. Torquato, *Random Heterogeneous Materials: Microstructure and Macroscopic Properties* (Springer-Verlag, New York, 2002).

34. J. Freitag, H. Eicken, *J. Glaciol.* **49**, 349 (2003).

35. K. M. Golden, A. L. Heaton, H. Eicken, V. I. Lytle, *Mechanics of Materials* **38**, 801 (2006).

36. C. Bock, H. Eicken, *Ann. Glaciol.* **40**, 179 (2005).

37. S. Torquato, D. C. Pham, *Phys. Rev. Lett.* **92**, 255505:1 (2004).

38. B. I. Halperin, S. Feng, P. N. Sen, *Phys. Rev. Lett.* **54**, 2391 (1985).

39. K. Golden, *Phys. Rev. Lett.* **65**, 2923 (1990).

40. B. Berkowitz, I. Balberg, *Transport in Porous Media* **9**, 275 (1992).